npj | clean water

www.nature.com/npjcleanwater

ARTICLE OPEN

Metal oxide single-component light-powered micromotors for photocatalytic degradation of nitroaromatic pollutants

Xia Peng[1], Mario Urso[1] and Martin Pumera[1,2,3,4]✉

Mass transfer is a key parameter in heterogeneous reactions. Micro/nanomachines, a promising technology for environmental applications, significantly enhance the performance of conventional purification treatments because of the active motion ability and thus enhanced diffusion (superdiffusion) of these photocatalysts, which in turn leads to dramatically improved mass transfer and higher degradation capability compared to stationary microparticles. However, the design of micromotors generally involves noble metals, for instance, Au and Pt, to achieve an effective autonomous motion. Considering the expensive fabrication cost and complicated steps, we present Pt-free single-component light-powered WO_3 micromotors capable of enhanced diffusion and effective degradation of nitroaromatic compounds in water. These microswimmers, synthesized by a hydrothermal method, which is highly scalable at low cost, followed by calcination, exhibit fuel-free light-driven motion due to asymmetric light irradiation. Picric acid (PA) and 4-nitrophenol (4-NP) were selected as representative nitroaromatic contaminants and photocatalytically decomposed by WO_3 micromotors thanks to the close contact with the micromotors promoted by their self-propulsion. This work provides a low-cost, sustainable, scalable method for enhancing mass transfer by creating moving catalysts with broad application potential for water cleanup.

npj Clean Water (2023)6:21 ; https://doi.org/10.1038/s41545-023-00235-z

INTRODUCTION

Nitroaromatic compounds are organic composites that comprise one or more nitro groups (-NO_2) connected to the aromatic ring[1]. Taking advantage of these groups, nitroaromatic compounds have been broadly applied to fabricate diverse industrial products, such as explosives, pesticides, and dyes[2]. Unfortunately, the nitro group also hinders the biodegradation of these compounds, resulting in continuous environmental accumulation. Indeed, their extensive employment has led to severe contamination of groundwater and soil, which is usually associated with drinking water quality, severely posing a threat to human health[3,4]. Traditional wastewater purification approaches mainly depend on biological oxidation and physical procedures (i.e., activated carbon adsorption, nano-filtration)[5–7]. The biological process is inadequate as these compounds are barely degraded due to their high constancy in the water system. Physical methods only transfer the pollutants instead of destructive removal, which indicates that further treatments are necessary. Advanced oxidation processes (AOPs) have been extensively explored in degrading organic contaminations in wastewater[8–10]. AOPs generally involve highly reactive oxygen species (ROS), for instance, hydroxyl radical (•OH) and superoxide radical ($\bullet O_2^-$), which can oxidize hazardous chemical species in water[11]. Photocatalysis is a promising light-driven AOP technology, necessitating a photocatalyst and proper light irradiation to generate ROS that break down organic pollutants. Recently, nanostructured TiO_2, ZnO, and Fe_2O_3 photocatalysts have received great interest[12–17]. For instance, Reddy et al. proposed Cu-doped ZnO nanoparticles for RhB dye degradation under light irradiation[18]. Similarly, Z-scheme binary heterostructured nanocomposites (i.e., MoS_2/g-C_3N_4 and $ZnWO_4$/$NiFe_2O_4$) were employed for the efficient photocatalytic degradation of toxic organic pollutants[19,20]. However, these approaches are restricted because of the passive diffusion of photocatalytic materials, requiring constant agitation. Furthermore, most of them involved more than one component. Consequently, it is highly desirable to explore more facile and practical strategies to facilitate the removal of pollutants.

Light-powered micromotors, micro/nano-sized materials that exploit energy from a powerful, renewable, and abundant source, such as light, and convert it into motion, have received considerable interest[21–26]. Previous research has shown that the active locomotion of light-powered micromotors based on photocatalytic materials can overcome the limitation of passive diffusions of photocatalysts by enhancing the interactions with targeted pollutants[27–31]. For instance, Ma et al. developed tubular micromotors based on TiO_2, magnetic Fe_3O_4 nanoparticles, and Pt for the effective degradation of rhodamine 6G[30]. Moreover, light-powered ZnO/Pt micromotors with H_2O_2-free light-driven propulsion ability and hematite/Pt Janus microrobots were explored for nitroaromatic explosives decomposition[31,32]. However, a noble metal coating was required in both cases to unlock the self-propulsion ability, increasing fabrication costs and complexity. Therefore, low-cost and simpler micromotors remain to be explored for future practical applications.

Here, we demonstrate the photocatalytic degradation of nitroaromatic pollutants by noble metal-free single-component light-powered WO_3 micromotors. Compared to Au-WO_3@C Janus micromotors proposed by Ren et al. for the photodegradation of dye pollutants[25], single-component WO_3 micromotors without the need for additional noble-metal coating were prepared by a facile hydrothermal reaction followed by a calcination process. Once exposed to asymmetric light illumination, the micromotors

[1]Future Energy and Innovation Laboratory, Central European Institute of Technology, Brno University of Technology, Purkynova 123, 61200 Brno, Czech Republic. [2]Department of Medical Research, China Medical University Hospital, China Medical University, No. 91 Hsueh-Shih Road, TW-40402 Taichung, Taiwan. [3]Faculty of Electrical Engineering and Computer Science, VSB - Technical University of Ostrava, 17. listopadu 2172/15, 70800 Ostrava, Czech Republic. [4]Department of Chemical and Biomolecular Engineering, Yonsei University, 50 Yonsei-ro, Seodaemun-gu, Seoul 03722, Korea. ✉email: martin.pumera@ceitec.vutbr.cz

can exhibit fuel-free self-actuation in pure water, with remote control and rapid response over on/off switching of UV-light. Motion behavior in different conditions demonstrated that H_2O_2 enhanced the motion and diffusion of micromotors. Finally, these WO_3 micromotors were applied for the effective photodegradation of nitroaromatic compounds, among which picric acid (PA) and 4-nitrophenol (4-NP) were selected as models because of their hazardous nature and high stability in water. Such simple and low-cost micromotors capable of degrading toxic substances hold great potential in the micro/nanomotors systems for environmental remediation.

RESULTS

Characterization of WO_3 micromotors

WO_3 micromotors were successfully prepared via the combination of a simple hydrothermal method and a calcination process, as described in Fig. 1a. Specifically, a homogenous solution consisting of the tungsten precursor and glucose was sealed under the hydrothermal condition, followed by an annealing process in air to promote the formation of single-component WO_3 micromotors. Scanning electron microscopy (SEM) images in Fig. 1b illustrate the obtainment of WO_3 microspheres with sizes varying from 1 to 2 μm. A more detailed analysis displays a highly rough surface, ascribed to a hierarchical structure composed of assembled nanoparticles (Fig. 1c). Energy-dispersive X-ray spectroscopy (EDX) elemental mapping images validate the existence and even distribution of the W and O elements, as shown in Fig. 1d, e. The X-ray diffraction (XRD) pattern of WO_3 micromotors is displayed in Fig. 1f, which agrees with the standard monoclinic phase (JCPDS 83-0951)[33]. In fact, diffraction peaks are observed at $2\theta = 22.9°$, 23.4°, 24.1°, 26.4°, 28.1°, 32.8°, 33.1°, 41.6°, 50,43° and associated with the (002), (020), (200), (120), (112), (022), (202), (222), and (400) crystalline planes of WO_3. The chemical states of WO_3 micromotors were additionally determined by X-ray photoelectron spectroscopy (XPS). Figure 1g shows the main peaks ascribed to W 4*f* and O 1*s*, highlighted in the XPS wide spectrum. The high-resolution spectrum of W 4*f* demonstrates two distinguished peaks in Fig. 1g. The binding energies of W $4f_{7/2}$ and W $4f_{5/2}$, positioned at 35.3 eV and 37.3 eV, respectively, match well with reported values of the W^{6+} oxidation state for WO_3 microspheres. The high-resolution spectrum of O 1*s* displays two peaks at 531.8

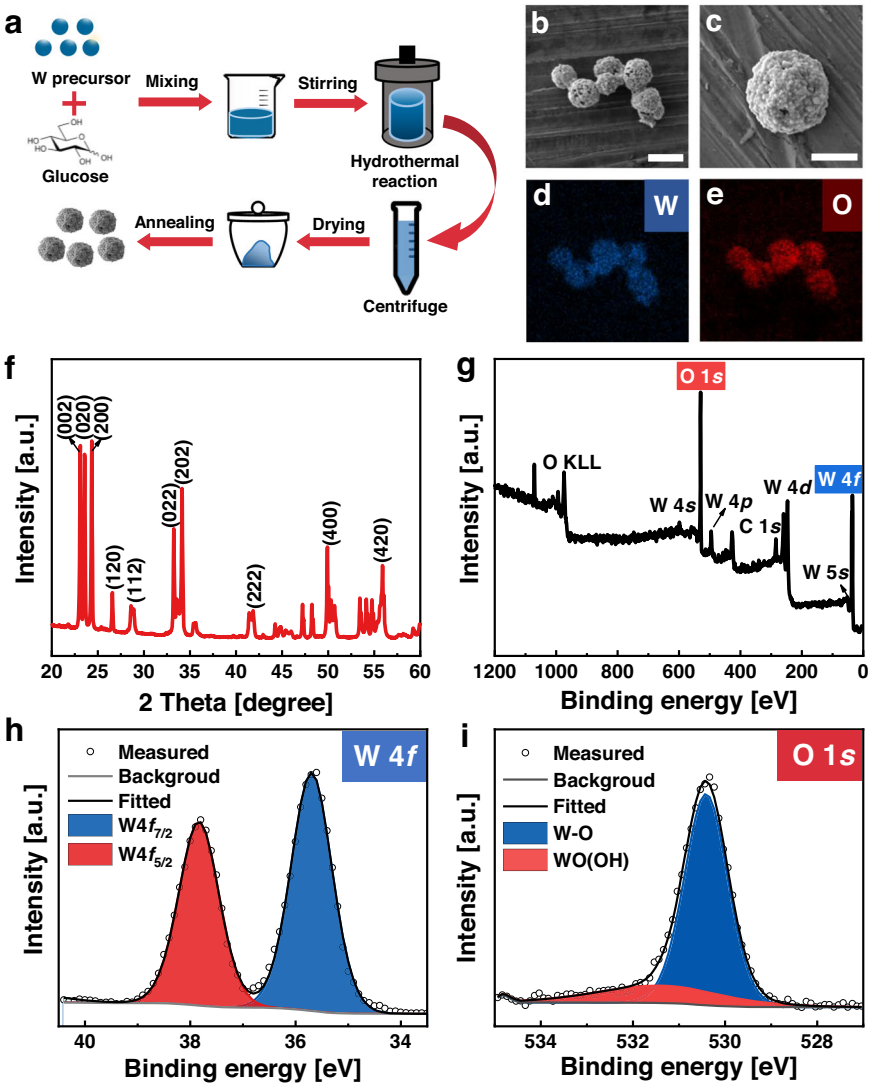

Fig. 1 The preparation process and characterization of WO_3 micromotors. a Schematic illustration of the preparation of WO_3 microspheres by hydrothermal and calcination processes. **b** (the scale bar is 2 μm) and **c** (the scale bar is 1 μm) SEM images of WO_3 micromotors. Elemental mapping images for **d** W and **e** O. **f** XRD pattern. **g** XPS wide spectrum. **h** High-resolution W 4*f* XPS spectrum. **i** High-resolution O 1*s* XPS spectrum.

and 530.3 eV binding energy (Fig. 1i)[34]. The peak at 531.8 eV is ascribed to OH groups on the WO_3 micromotors' surface, and the other peak agrees with the lattice oxygen in the crystal structure of WO_3 micromotors.

Motion behavior of WO_3 micromotors

The single-component WO_3 micromotors display autonomous motion when exposed to UV-light illumination both in fuel-free and H_2O_2 solutions. Previous research has elucidated the locomotion mechanism of single-constituent photocatalytic micromachines under light irradiation[35,36]. As illustrated in Fig. 2a, the incidence of photons with higher energy than the optical bandgap of WO_3 micromotors triggers the generation of electron-hole pairs. According to previous works[37–39], the edge of the conduction band (CB) of WO_3 micromotors ($E_{CB} = 0.77$ V_{NHE}, where E_{CB} is the conduction band edge at the normal hydrogen electrode (NHE)) lies below the photocatalytic hydrogen evolution threshold. The photogenerated electrons in the CB could not react with H^+ to generate H_2, whereas they can decompose H_2O or H_2O_2 in protons (H^+). Meanwhile, the photogenerated holes in the valence band (VB) can contribute to breaking down H_2O or H_2O_2 into •OH, O_2, and H^+. The non-uniform light exposure of WO_3 micromotors results in an asymmetrical generation of these chemical species, establishing a product gradient leading to their movement by self-phoresis[40,41]. An optical bandgap of 2.72 eV, representing the minimum energy to excite the electrons from the VB to the CB, was determined from the absorption spectrum of WO_3 micromotors (Fig. 2b) using the Tauc plot (inset in Fig. 2b)[42]. Figure 2c exhibits the time-lapse images of a WO_3 micromotor's trajectory at intervals of ~5 s in pure water and 1% H_2O_2 (Supplementary Videos 1 and 2). WO_3 micromotors exhibit Brownian motion without light and fuel-free propulsion when illuminated by UV-light. A longer trajectory can be observed when 1% H_2O_2 is introduced due to the more pronounced product gradient around the micromotor. The corresponding speeds of these micromotors are also depicted in Fig. 2d and Supplementary Fig. 1a, further indicating the light-controlled on/off movement in pure water and H_2O_2.

The motion of WO_3 micromotors under different conditions was further studied by calculating the mean squared displacement (MSD). As reported in Fig. 2e, the MSD of WO_3 micromotors in 1% H_2O_2 without UV-light irradiation follows a linear increase within 1 s, indicating merely Brownian motion. The same is observed for the micromotors in pure water (Supplementary Fig. 1b). When UV-light is involved, the MSD of micromotors in pure water and H_2O_2 manifests a parabolic increase with time owing to the light-induced micromotors' self-propulsion (Fig. 2e and Supplementary Fig. 1b)[32,43,44]. According to MSD analyses, the diffusion coefficients (D) of WO_3 micromotors were plotted and inserted in Fig. 2e. Under UV-light irradiation in pure water, D is up to 2.0 ± 0.1 $\mu m^2 s^{-1}$, whereas a tenfold increase is noted in 1% H_2O_2 (20 ± 1 $\mu m^2 s^{-1}$). To study the parameters that regulate the photocatalytic locomotion of WO_3 micromotors, different concentrations of H_2O_2 were introduced, as depicted in Fig. 2f. The speed of micromotors was progressively increased from 5 ± 1 $\mu m\ s^{-1}$ to 26 ± 2 $\mu m\ s^{-1}$ as a higher concentration of H_2O_2 (1% H_2O_2) was added.

Nitroaromatic pollutants degradation

Water contamination caused by nitroaromatic compounds poses severe environmental hazards due to their wide usage for the manufacture of explosives, pesticides, and pharmaceuticals and their non-biodegradable nature with high persistence[2]. Recently, various environmentally friendly treatments that employ active propelled micro/nanomotors have been demonstrated for the degradation or absorption of nitroaromatic compounds[6,45–48]. Nevertheless, most micromotors involve a primary half-coating with expensive Pt or Au to achieve the asymmetrical structure for light-activated propulsion or chemically-driven motion based on H_2O_2 decomposition. There is a strong desire to develop easily fabricated, low-cost, and recyclable micromotors as candidates to facilitate their practical applications. Therefore, we employed the single-component WO_3 micromotors to degrade nitroaromatic compounds in water. PA and 4-NP (molecular structures in the insets in Figs. 3a and 4, respectively) were both selected as representative nitroaromatic contaminants. PA was also employed to investigate the reusability and photodegradation mechanism of WO_3 micromotors.

PA photocatalytic degradation capability of WO_3 micromotors was estimated under UV-light irradiation up to 2 h in 1% H_2O_2. Figure 3a shows the UV-Vis spectra of PA solutions at different reaction times. The intensity of the absorbance peak after the treatments with micromotors decreases with time, suggesting the degradation of PA. The degradation efficiency of micromotors was estimated according to Eq. (1)

$$\text{Degradation Efficiency} = \frac{C_0 - C_t}{C_0} \times 100\% \quad (1)$$

where C_0 represents the original PA concentration, while C_t is the PA concentration at the time t. Specifically, the decomposition efficiency of PA is 72% after 2 h treatment, as shown in Fig. 3c (red line). Additionally, several control experiments were accomplished to assess other contributions to the PA photocatalytic degradation using WO_3 micromotors: 1) PA + UV-light; 2) PA + UV-light + H_2O_2; 3) PA + H_2O_2; 4) PA + WO_3 + UV-light; 5) PA + WO_3 + H_2O_2. As shown in Supplementary Fig. 2a, negligible decreases in the peak intensity can be observed after 2 h photodegradation without micromotors. For fuel-free motion (PA + WO_3 + UV-light) and no motion (PA + WO_3 + H_2O_2), the degradation efficiencies are merely 28% and 5%, respectively, which are lower than the efficient motion with H_2O_2 (PA + WO_3 + UV-light + H_2O_2). These results suggest that UV-light and the addition of H_2O_2 are not sufficient to degrade PA. The reusability of materials has been considered one of the most critical factors for their practical applications. Figure 3b shows that the degradation efficiency still exhibits up to 55% after several consecutive degradation cycles (Supplementary Fig. 2b), which indicates that these micromotors preserved their high photocatalytic capability.

Photogenerated radicals (i.e., h^+, •OH, O_2^-) are crucial for degrading organic pollutants. Owing to the low CB position of WO_3 micromotors ($E_{CB} = 0.77$ V_{NHE}), the reduction of O_2 ($O_2 + e^- \rightarrow {}^\bullet O_2^-$ (aq), −0.33 V_{NHE}) cannot happen under light irradiation[37]. Consequently, photogenerated h^+ and •OH are considered the main radicals that can break down PA. Upon UV-light irradiation, •OH radicals can be formed in two paths: the oxidation of water and reduction of H_2O_2 adsorbed on the surface of WO_3 micromotors as follows.

$$H_2O + h^+ \rightarrow {}^\bullet OH + H^+ \quad (2)$$

$$H_2O_2 + e^- \rightarrow {}^\bullet OH + OH^- \quad (3)$$

A suitable potential value for the reduction of H_2O_2 is $E_{CB} = 0.87$ V_{NHE}[49]. WO_3 has a higher E_{CB} (0.77 V_{NHE}), so this reaction can happen due to being energetically favorable. Therefore, the enhanced photodegradation efficiency achieved by PA + WO_3 + UV-light + H_2O_2 relies on the photocatalytic capability of WO_3 micromotors and also the enhanced radical production on the surface of WO_3 micromotors because of the presence of H_2O_2. In order to further understand the degradation mechanism, radical trapping experiments were performed[50]. In this regard, EDTA (10 mg L^{-1}) and isopropanol (0.25 µL mL^{-1}) were chosen as typical scavengers to capture h^+ and •OH, respectively[51]. As shown in Fig. 3c, the involvement of isopropanol sharply decreased the photo-induced degradation efficiency of the micromotors,

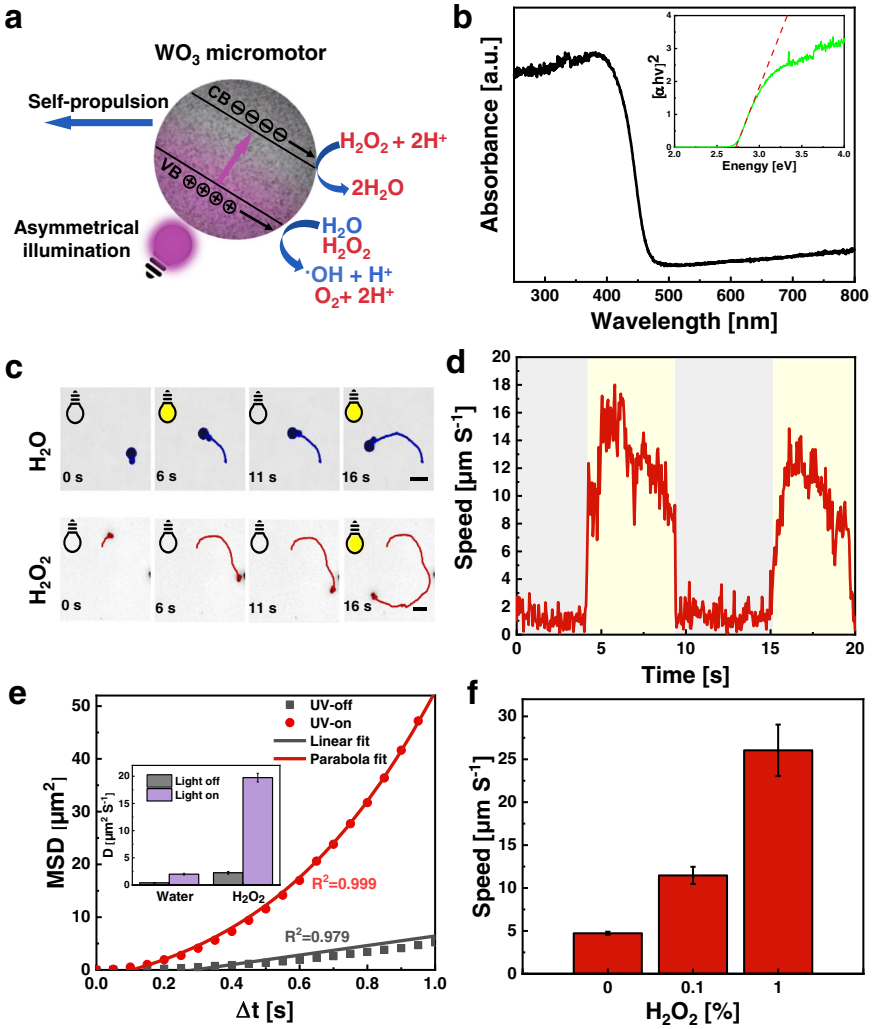

Fig. 2 Motion behavior of WO_3 micromotors. a Schematic illustration of the propulsion mechanism of light-powered WO_3 micromotors. **b** UV-Vis spectrum of WO_3 micromotors. The inset shows the bandgap estimation from the corresponding Tauc plot. **c** Time-lapse images of a WO_3 micromotor in 1% H_2O_2 at intervals of ~5 s. Scale bars are 5 μm. **d** Instantaneous speed values and **e** MSD plots of WO_3 micromotors in 1% H_2O_2 without/with UV-light irradiation. The inset shows the corresponding diffusion coefficients according to MSD plots fitting. **f** Comparison of micromotors' speed in different concentrations of H_2O_2. Error bars represent the standard deviation, $n = 5$ independent replicates.

resulting in 37% (Supplementary Fig. 3b). Therefore, the addition of isopropanol decreased the amount of free •OH species, resulting in a markable decrease in the PA photodegradation efficiency. On the contrary, the addition of EDTA accelerated the photodegradation process, enhancing the photoactivity of the micromotors after 2 h light exposure with 1% H_2O_2 (Supplementary Fig. 3a). On these bases, it can be concluded that the radicals •OH are the key photogenerated chemical species responsible for PA oxidation (Fig. 3d).

4-Nitrophenol (4-NP) is a poisonous and bio-rebellious nitroaromatic contaminant that can harm human health considerably[8]. In this work, WO_3 micromotors were also used to degrade 4-NP. Initially, control experiments were run to exclude the interference of other factors (UV-light, H_2O_2, and their combination). As depicted in Supplementary Fig. 4a, no noticeable decline in the absorbance intensity can be observed when micromotors are not involved in control experiments. Figure 4 demonstrates the 4-NP degradation after the treatment with WO_3 micromotors under light exposure in water (free-fuel motion) and in the presence of H_2O_2 (fuel-driven motion) for different durations. Obviously, micromotors powered by the fuel presented an enhanced degradation activity, resulting in an efficiency of 40%, higher than fuel-free motion (11%). This phenomenon can be explained by the lower propulsion speed of micromotors in pure water without any agitation.

DISCUSSION

Here, we reported the large-scale synthesis of precious metal-free single-component WO_3 micromotors via a facile hydrothermal method, which is easily scalable, combined with calcination. We demonstrated that such WO_3 micromachines exhibit self-propulsion upon light exposure, even without H_2O_2 fuel. Specifically, they displayed perceptive on/off motion capability with light exposure. From MSD analyses, it can be proved that micromotors showed pure Brownian motion without light, whereas self-propulsion was achieved under asymmetric UV illumination. The active motion and photocatalytic activity of WO_3 micromotors were applied to degrade toxic nitroaromatic pollutants, such as PA and 4-NP. The micromotors degraded 70% of PA and 40% of 4-NP in water without any external agitation. The photodegradation mechanism was also investigated through radical trapping experiments, which confirmed that •OH is the key ROS responsible for pollutant degradation. The obtained results indicate the possibility of using single-component

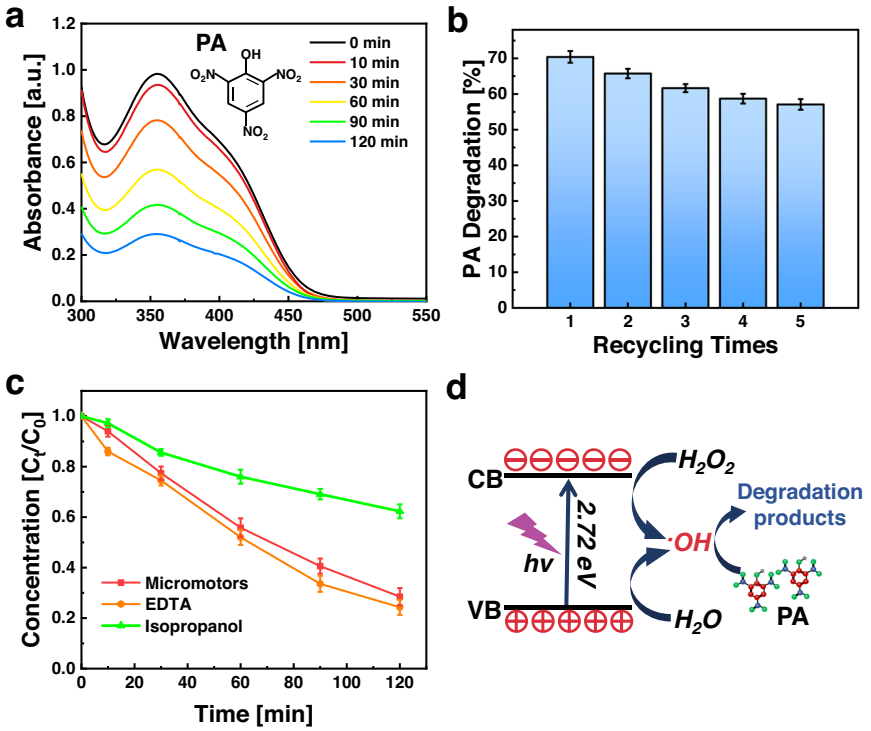

Fig. 3 Photocatalytic degradation of PA by WO_3 micromotors. a UV-Vis spectra of PA after photocatalytic degradation by WO_3 micromotors exposed to UV-light irradiation in 1% H_2O_2; **b** Reusability assessment of WO_3 micromotors under 5 successive cycles of PA degradation; **c** Radical scavenger experiments conducted by employing EDTA and isopropanol; **d** Proposed WO_3 photodegradation mechanism. Error bars represent the standard deviation, $n = 3$ independent replicates.

photocatalytic micromotors to eliminate non-biodegradable and hazardous pollutants from industrial sewages.

METHODS

Synthesis of WO_3 micromotors

Firstly, 50 mL of deionized (DI) water was placed in an 80 mL beaker. Then, 1 mmol Na_2WO_4 was dissolved in the prepared DI water with constant magnetic stirring. Afterward, 25 mmol of glucose was added to the prepared suspension. The final mixture was magnetically mixed until obtaining a homogeneous solution. Then, the solution was transferred into an autoclave. The autoclave was sealed and placed in a preheated oven at 200 °C and lasted for 20 h. When the reaction ended, the autoclave was taken out from the oven and naturally cooled down to room temperature. The precipitated product was cleaned using DI water and ethanol and dried in an oven overnight. Then, the dried products were sealed with aluminum foil and calcined at 550 °C in air. The obtained green-colored product was collected for further experiments.

Characterization of micromotors

SEM images of WO_3 micromotors were acquired by a Tescan MIRA 3 XMU instrument. EDX mapping analysis was conducted by an EDX detector (Oxford Instruments) coupled to the SEM. The chemical states of WO_3 micromotors were characterized by a Kratos Analytical Axis Supra instrument.

Motion experiments

The micromotors' motion was recorded by an inverted microscope (Nikon ECLIPSE Ts2R) and a camera (BASLER acA1920-155uc). Specifically, a 5 µL aqueous suspension containing WO_3 micromotors was used for motion experiments. Three

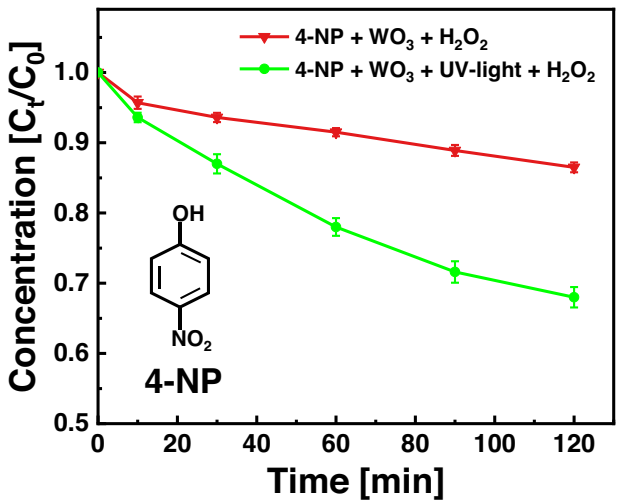

Fig. 4 Photocatalytic degradation of 4-NP using WO_3 micromotors under UV-light irradiation in 1% H_2O_2. Error bars represent the standard deviation, $n = 3$ independent replicates.

concentrations of H_2O_2 (Merck, 30%) were mixed with the previous suspension, achieving final concentrations of 0, 0.1, and 1%, to observe and record the videos of micromotors' motion with a frame rate of 25 fps. No surfactants were involved in all experiments. The micromotors were exposed to a UV-light source (Cool LED pE-100, 1.6 W cm^{-2}) with a 365 nm wavelength. In order to observe the on/off behavior of micromotors, the light source was switched on/off at defined time intervals (~5 s). The WO_3 micromotors' velocities and trajectories were calculated from the recorded videos and tracked by the NIS Elements Advanced Research software. The diffusion coefficient of micromotors was

calculated according to the following equations based on the results of MSD plot fitting:

$$\mathrm{MSD} = 4D\Delta t \quad (4)$$

$$\mathrm{MSD} = 4D\Delta t + v^2\Delta t^2 \quad (5)$$

Pollutants degradation experiments

In all experiments, 2 mg mL^{-1} of micromotors, 50 μM aqueous solution of picric acid (PA, Merck, 99%), and 1% H_2O_2 were consecutively placed in UV-transparent cuvettes. Once UV-light (356 nm, 9 W) was turned on, the cuvettes were put in a closed box for in total of 120 min. Control experiments without UV-light irradiation or H_2O_2 were performed to elucidate the contribution of micromotors. After a different light exposure time, the mixtures were centrifuged at a certain speed for 3 min to obtain the final solution without the micromotors. A UV-Vis spectrophotometer (Jasco V-750) was used to measure the absorbance spectra of the solutions. The absorbance peak at 354 nm was considered to calculate the degradation efficiency. The degradation of 150 μM 4-nitrophenol (4-NP, Sigma Aldrich, 99%) followed the same procedures as PA.

DATA AVAILABILITY

The data that support the findings of this study are available from the corresponding author upon reasonable request.

Received: 17 August 2022; Accepted: 20 February 2023;
Published online: 14 March 2023

REFERENCES

1. Kovacic, P. & Somanathan, R. Nitroaromatic compounds: environmental toxicity, carcinogenicity, mutagenicity, therapy and mechanism. *J. Appl. Toxicol.* **34**, 810–824 (2014).
2. Ju, K. S. & Parales, R. E. Nitroaromatic compounds, from synthesis to biodegradation. *Microbiol. Mol. Biol. Rev.* **74**, 250–272 (2010).
3. Tiwari, J., Tarale, P., Sivanesan, S. & Bafana, A. Environmental persistence, hazard, and mitigation challenges of nitroaromatic compounds. *Environ. Sci. Pollut. Res.* **26**, 28650–28667 (2019).
4. Cai, Q. Y., Mo, C. H., Wu, Q. T., Zeng, Q. Y. & Katsoyiannis, A. Occurrence of organic contaminants in sewage sludges from eleven wastewater treatment plants. *Chemosphere* **68**, 1751–1762 (2007).
5. Jurado-Sánchez, B. & Wang, J. Micromotors for environmental applications: a review. *Environ. Sci. Nano* **5**, 1530–1544 (2018).
6. Oral, C. M., Ussia, M. & Pumera, M. Self-propelled activated carbon micromotors for 'on-the-fly' capture of nitroaromatic explosives. *J. Phys. Chem. C* **125**, 18040–18045 (2021).
7. Chan, S. S., Khoo, K. S., Chew, K. W., Ling, T. C. & Show, P. L. Recent advances biodegradation and biosorption of organic compounds from wastewater: microalgae-bacteria consortium - a review. *Bioresour. Technol.* **344**, 126159 (2022).
8. Patial, S. et al. Recent advances in photocatalytic multivariate metal organic frameworks-based nanostructures toward renewable energy and the removal of environmental pollutants. *Mater. Today Energy* **19**, 100589 (2021).
9. Hasija, V. et al. Advanced activation of persulfate by polymeric G-C_3N_4 based photocatalysts for environmental remediation: a review. *J. Hazard. Mater.* **413**, 125324 (2021).
10. Sharma, S. et al. Tailoring cadmium sulfide-based photocatalytic nanomaterials for water decontamination: a review. *Environ. Chem. Lett.* **19**, 271–306 (2021).
11. Liu, H., Wang, C. & Wang, G. Photocatalytic advanced oxidation processes for water treatment: recent advances and perspective. *Chem. Asian J.* **15**, 3239–3253 (2020).
12. Zhao, B. et al. Degradation of 4-nitrophenol (4-NP) using Fe-TiO_2 as a heterogeneous photo-Fenton catalyst. *J. Hazard. Mater.* **176**, 569–574 (2010).
13. Ussia, M. et al. Light-propelled nanorobots for facial titanium implants biofilms removal. *Small* **18**, 2200708 (2022).
14. Hitam, C. N. C. & Jalil, A. A. A review on exploration of Fe_2O_3 photocatalyst towards degradation of dyes and organic contaminants. *J. Environ. Manag.* **258**, 110050 (2019).
15. Chen, X., Wu, Z., Liu, D. & Gao, Z. Preparation of ZnO photocatalyst for the efficient and rapid photocatalytic degradation of azo dyes. *Nanoscale Res. Lett.* **12**, 4–13 (2017).
16. Karthik, K. V. et al. Barium titanate nanostructures for photocatalytic hydrogen generation and photodegradation of chemical pollutants. *J. Mater. Sci. Mater. Electron.* **30**, 20646–20653 (2019).
17. Urso, M., Ussia, M. & Pumera, M. Smart micro- and nanorobots for water purification. *Nat. Rev. Bioeng.* https://doi.org/10.1038/s44222-023-00025-9 (2023).
18. Karthik, K. V. et al. Green synthesis of Cu-doped ZnO nanoparticles and its application for the photocatalytic degradation of hazardous organic pollutants. *Chemosphere* **287**, 132081 (2022).
19. Monga, D., Ilager, D., Shetti, N. P., Basu, S. & Aminabhavi, T. M. 2D/2d heterojunction of MoS_2/g-C_3N_4 nanoflowers for enhanced visible-light-driven photocatalytic and electrochemical degradation of organic pollutants. *J. Environ. Manag.* **274**, 111208 (2020).
20. Reddy, C. V. et al. Z-Scheme binary 1D $ZnWO_4$ nanorods decorated 2D $NiFe_2O_4$ nanoplates as photocatalysts for high efficiency photocatalytic degradation of toxic organic pollutants from wastewater. *J. Environ. Manag.* **268**, 110677 (2020).
21. Xu, L., Mou, F., Gong, H., Luo, M. & Guan, J. Light-driven micro/nanomotors: from fundamentals to applications. *Chem. Soc. Rev.* **46**, 6905–6926 (2017).
22. Vizsnyiczai, G. et al. Light controlled 3D micromotors powered by bacteria. *Nat. Commun.* **8**, 15974 (2017).
23. Dong, R. et al. Visible-light-driven BiOI-based Janus micromotor in pure water. *J. Am. Chem. Soc.* **139**, 1722–1725 (2017).
24. Peng, X., Urso, M., Ussia, M. & Pumera, M. Shape-controlled self-assembly of light-powered microrobots into ordered microchains for cells transport and water remediation. *ACS Nano* **16**, 7615–7625 (2022).
25. Zhang, Q. et al. Light-driven Au-WO_3@C Janus micromotors for rapid photodegradation of dye pollutants. *ACS Appl. Mater. Interfaces* **9**, 4674–4683 (2017).
26. Urso, M., Ussia, M., Novotný, F. & Pumera, M. Trapping and detecting nanoplastics by MXene-derived oxide microrobots. *Nat. Commun.* **13**, 3573 (2022).
27. Ussia, M. et al. Active light-powered antibiofilm ZnO micromotors with chemically programmable properties. *Adv. Funct. Mater.* **31**, 2101178 (2021).
28. Fernández-Medina, M., Ramos-Docampo, M. A., Hovorka, O., Salgueiriño, V. & Städler, B. Recent advances in nano- and micromotors. *Adv. Funct. Mater.* **30**, 1908283 (2020).
29. Urso, M., Ussia, M. & Pumera, M. Breaking polymer chains with self-propelled light-controlled navigable hematite microrobots. *Adv. Funct. Mater.* **31**, 2101510 (2021).
30. Liang, C. et al. Bilayer tubular micromotors for simultaneous environmental monitoring and remediation. *ACS Appl. Mater. Interfaces* **10**, 35099–35107 (2018).
31. Ying, Y. et al. Light-driven ZnO brush-shaped self-propelled micromachines for nitroaromatic explosives decomposition. *Small* **16**, 1902944 (2020).
32. Peng, X., Urso, M. & Pumera, M. Photo-Fenton degradation of nitroaromatic explosives by light-powered hematite microrobots: when higher speed is not what we go for. *Small Methods* **5**, 2100617 (2021).
33. Szilágyi, I. et al. WO_3 photocatalysts: Influence of structure and composition. *J. Catal.* **294**, 119–127 (2012).
34. Kalanur, S. S. Structural, optical, band edge and enhanced photoelectrochemical water splitting properties of tin-doped WO_3. *Catalysts* **9**, 456 (2019).
35. Hong, Y., Diaz, M., Córdova-Fteueroa, U. M. & Sen, A. Light-driven titanium-dioxide-based reversible microfireworks and micromotor/micropump systems. *Adv. Funct. Mater.* **20**, 1568–1576 (2010).
36. Villa, K., Děkanovský, L., Plutnar, J., Kosina, J. & Pumera, M. Swarming of perovskite-like Bi_2WO_6 microrobots destroy textile fibers under visible light. *Adv. Funct. Mater.* **30**, 2007073 (2020).
37. Mardare, C. C. & Hassel, A. W. Review on the versatility of tungsten oxide coatings. *Phys. Status Solidi A* **216**, 1900047 (2019).
38. Nguyen, T. T., Nam, S. N., Son, J. & Oh, J. Tungsten trioxide (WO_3)-assisted photocatalytic degradation of amoxicillin by simulated solar irradiation. *Sci. Rep.* **9**, 9349 (2019).
39. Xiao, T. et al. In situ construction of hierarchical WO_3/g-C_3N_4 composite hollow microspheres as a Z-scheme photocatalyst for the degradation of antibiotics. *Appl. Catal. B Environ.* **220**, 417–428 (2018).
40. Pourrahimi, A. M., Villa, K., Ying, Y., Sofer, Z. & Pumera, M. ZnO/ZnO_2 /Pt Janus micromotors propulsion mode changes with size and interface structure: enhanced nitroaromatic explosives degradation under visible light. *ACS Appl. Mater. Interfaces* **10**, 42688–42697 (2018).
41. Ibele, M., Mallouk, T. E. & Sen, A. Schooling behavior of light-powered autonomous micromotors in water. *Angew. Chem. Int. Ed.* **48**, 3308–3312 (2009).
42. Vemuri, R. S., Engelhard, M. H. & Ramana, C. V. Correlation between surface chemistry, density, and band gap in nanocrystalline WO_3 thin films. *ACS Appl. Mater. Interfaces* **4**, 1371–1377 (2012).
43. Hu, Y., Liu, W. & Sun, Y. Self-propelled micro-/nanomotors as 'on-the-move' platforms: cleaners, sensors, and reactors. *Adv. Funct. Mater.* **32**, 2109181 (2022).

44. Gao, C., Feng, Y., Wilson, D. A., Tu, Y. & Peng, F. Micro-nano motors with taxis behavior: principles, designs, and biomedical applications. *Small* **18**, 2106263 (2022).
45. Kong, L., Ambrosi, A., Nasir, M. Z. M., Guan, J. & Pumera, M. Self-propelled 3D-printed 'aircraft carrier' of light-powered smart micromachines for large-volume nitroaromatic explosives removal. *Adv. Funct. Mater.* **29**, 1903872 (2019).
46. Srivastava, S. K., Guix, M. & Schmidt, O. G. Wastewater mediated activation of micromotors for efficient water cleaning. *Nano Lett.* **16**, 817–821 (2016).
47. Mayorga-Martinez, C. C., Vyskočil, J., Novotný, F. & Pumera, M. Light-driven Ti_3C_2 MXene micromotors: Self-propelled autonomous machines for photodegradation of nitroaromatic explosives. *J. Mater. Chem. A* **9**, 14904–14910 (2021).
48. Kong, L., Mayorga-Martinez, C. C., Guan, J. & Pumera, M. Fuel-free light-powered TiO_2/Pt Janus micromotors for enhanced nitroaromatic explosives degradation. *ACS Appl. Mater. Interfaces* **10**, 22427–22434 (2018).
49. Kochergin, Y. S., Villa, K., Nemeškalová, A., Kuchař, M. & Pumera, M. Hybrid inorganic-organic visible-light-driven microrobots based on donor-acceptor organic polymer for degradation of toxic psychoactive substances. *ACS Nano* **15**, 18458–18468 (2021).
50. Hirakawa, T. & Nosaka, Y. Properties of $O_2^{\bullet-}$ and •OH formed in TiO_2 aqueous suspensions by photocatalytic reaction and the influence of H_2O_2 and some ions. *Langmuir* **18**, 3247–3254 (2002).
51. Liu, T. et al. Comparative study of the photocatalytic performance for the degradation of different dyes by $ZnIn_2S_4$: Adsorption, active species, and pathways. *RSC Adv.* **7**, 12292–12300 (2017).

ACKNOWLEDGEMENTS

M.P. acknowledges the financial support of the Grant Agency of the Czech Republic (EXPRO: 19-26896X). X.P. was supported by the China Scholarship Council (CSC No. 202008320382). CzechNanoLab project LM2018110 funded by MEYS CR is gratefully acknowledged for the financial support of the measurements/sample fabrication at CEITEC Nano Research Infrastructure.

AUTHOR CONTRIBUTIONS

X.P. prepared, and characterized the micromotors, evaluated the performance of the motion, conducted the degradation experiments, and wrote the manuscript. M.U. designed the experiments and contributed to data interpretation. X.P. and M.P. originated the idea. M.U. and M.P. supervised the research. All authors have given approval to the final version of the manuscript.

COMPETING INTERESTS

The authors declare no competing interests.

ADDITIONAL INFORMATION

Supplementary information The online version contains supplementary material available at https://doi.org/10.1038/s41545-023-00235-z.

Correspondence and requests for materials should be addressed to Martin Pumera.

Reprints and permission information is available at http://www.nature.com/reprints

Publisher's note Springer Nature remains neutral with regard to jurisdictional claims in published maps and institutional affiliations.